Two-flux tunable Aharonov-Bohm effect in a photonic lattice

V. Brosco and L. Pilozzi [*]

Institute for Complex Systems, National Research Council, Via dei Taurini 19, 00185 Rome, Italy
and Research Center Enrico Fermi, Via Panisperna 89a, 00184 Rome, Italy

C. Conti

Institute for Complex Systems, National Research Council, Via dei Taurini 19, 00185 Rome, Italy;
Department of Physics, University Sapienza, Piazzale Aldo Moro 5, 00185 Rome, Italy;
and Research Center Enrico Fermi, Via Panisperna 89a, 00184 Rome, Italy

We study the Aharonov-Bohm (AB) caging effect in a one-dimensional lattice of θ-shaped units defining a chain of interconnected plaquettes, each one threaded by two synthetic flux lines. In the proposed system, light trapping results from the destructive interference of waves propagating along three arms. This implies that the caging effect is tunable and it can be controlled by changing the tunnel couplings J. These features reflect on the diffraction pattern allowing us to establish a clear connection between the lattice topology and the resulting AB interference.

I. INTRODUCTION

In the early 1980's the geometrical interpretation of some phenomenological observables introduced a new paradigm for the explanation of different effects [1], modifying, for example, our view of nonrelativistic quantum phenomena such as the quantum Hall effect [2], and prompting new developments and discoveries of paramount relevance ranging from modern polarization theory [3] to topological phases [4].

Nowadays, the geometry of the Hilbert space, with its metric, defining the distance between two quantum states, and its connection [5], fixing the phase accumulated along quantum trajectories, is a central object in condensed matter research, holding great promise for quantum information applications. In photonics and atomic physics the quest to engineer and control the geometric and topological properties of artificial lattices fostered remarkable efforts to implement effective electromagnetic fields for neutral particles [6]. Just to mention a few examples, uniform magnetic fields were achieved in optical lattice-based experiments [7], in ring resonator arrays [8], and in optomechanical systems [9]. In photonic lattices, artificial gauge fields were generated using different techniques, i.e., introducing topological defects in two-dimensional structures [10,11], applying time-dependent modulation [12–14], employing synthetic modal dimensions [15], and, very recently, controlling the orbital angular momentum of the input light beam [16]. What underlies most of the observations carried out in the above systems is the first discovered and most basic consequence of the existence of gauge fields, the Aharonov-Bohm (AB) effect [17]. The paramount importance of this effect ranges from metrological applications to basic physics [18]. It is a nonlocal effect, arising from the inter-

ference of electron beams traveling along paths enclosing a magnetic flux. As first recognized by Wu and Yang [19], it naturally leads to the concept of a path-dependent phase factor as a basis to describe electromagnetism and gauge theories in general. Furthermore, as it clearly emerges in path-integral derivations, AB interference reflects the multiply connected nature of the space and it may have impressive consequences on transport. An example is Aharonov-Bohm caging, a single-particle localization effect arising from the interplay between the lattice structure and the magnetic flux, first predicted by Vidal *et al.* [20] for two-dimensional electronic lattices and for interacting particles in a one-dimensional periodic structure [21], and subsequently extended and experimentally verified in different contexts [22–25], including photonic lattices (see, e.g., Refs. [12,26–31]). It has been shown to occur for periodic lattices, such as the well-known rhombi chain (rc), when the magnetic flux per plaquette equals a given critical value $\phi_{\mathrm{rc}} = \phi_c$.

In the present paper we show that by properly engineering the lattice it is possible to tune the caging away from this critical value and control it by changing the lattice couplings. To this end we study the propagation of light through a one-dimensional array of θ-shaped plaquettes threaded by two fluxes as shown in Fig. 1(a), that, for brevity, we call the θ lattice. It reduces to the simple rhombi chain with only a single flux ϕ_{rc}, for specific couplings going to zero, as shown in Fig. 1(b). The presence of two fluxes in the θ lattice allows us to investigate, in a simple but nontrivial framework, the signatures of Aharonov-Bohm interference on diffraction patterns, highlighting its topological significance and showing how in this case the caging effect becomes fully tunable. As known, the AB is a topological effect in that it requires the particle to be confined to a multiply connected region where there is no way to relate a phase shift to any arm of the path: It depends only on the topology of the path with reference to
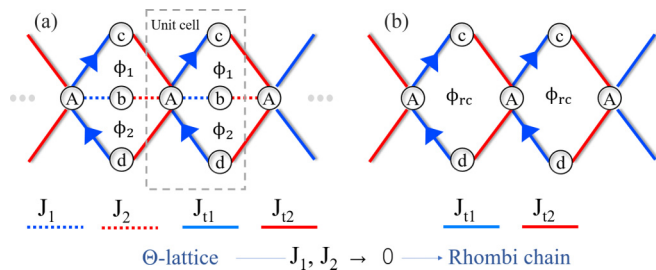
[*]laura.pilozzi@isc.cnr.it

FIG. 1. (a) Sketch of the structure of the θ lattice composed of interconnected plaquettes, each one threaded by two synthetic flux lines, ϕ_1 and ϕ_2. An arrow means a phase $e^{i\phi}$. Each plaquette shows three arms connecting the A site with respectively the b, c, and d ones. (b) For $J_1, J_2 = 0$ the θ lattice reduces to the rhombi chain (rc) with a single flux per plaquette ϕ_{rc}.

the enclosed flux. The presence of three arms and two fluxes allows us to better highlight this property with respect to the simple rhombi chain.

II. MODEL

We consider a one-dimensional lattice of θ-shaped units as shown in Fig. 1(a). Its unit cell consists of four sites indicated, respectively, as A, b, c, and d. The three arms of each ring, defined by the sites A_n, A_{n+1}, and respectively b_n, c_n, and d_n, enclose two synthetic flux lines, indicated respectively as ϕ_1 and ϕ_2.

The Hamiltonian of the θ lattice can thus be written as

$$H = \sum_n [J_{t1}(a_n^\dagger c_n e^{-i\phi_1} + a_n^\dagger d_n e^{i\phi_2}) + J_{t2}(a_n^\dagger d_{n-1} + a_n^\dagger c_{n-1})$$
$$+ J_1 a_n^\dagger b_n + J_2 a_n^\dagger b_{n-1} + \text{H.c.}], \quad (1)$$

where $m_n, m_n^\dagger$ with $m = a, b, c, d$ are bosonic annihilation and creation operators corresponding to the sites A, b, c, d of the cell n. Switching to k space we obtain

$$\mathcal{H}(k, \phi_1, \phi_2) = \sum_k [J_b(k) a_k^\dagger b_k + J_c(k, \phi_1) a_k^\dagger c_k$$
$$+ J_d(k, \phi_2) a_k^\dagger d_k + \text{H.c.}], \quad (2)$$

where $m_k = \frac{1}{\sqrt{N}} \sum_n m_n e^{ikn}$, with N denoting the number of unit cells in the lattice, while $J_b(k) = J_1 + J_2 e^{-ik}$ and $J_c(k, \phi) = J_d(k, -\phi) = J_{t1} e^{-i\phi} + J_{t2} e^{-ik}$, where J_1 and J_{t1} and J_2 and J_{t2} denote the intra- and intercell hopping amplitudes. The ϕ_1, ϕ_2 dependence of J_c and J_d is due to the presence of the synthetic gauge fields. We note that setting $J_{t1} = 0$, the θ lattice reduces to the non-Abelian Lieb lattice model [32] while setting $J_b = 0$ it reduces to the standard rhombi chain. The Hamiltonian $\mathcal{H}(k, \phi_1, \phi_2)$ is invariant, up to a gauge transformation, under permutations of the three arms b, c, and d, i.e., under elements of the non-Abelian group S_3. This implies that the state

$$|\phi_s(k)\rangle = J_b|b_k\rangle + J_c|c_k\rangle + J_d|d_k\rangle, \quad (3)$$

invariant under elements of S_3, yields two dispersive modes,

$$|\psi_\pm(k)\rangle = \frac{1}{\sqrt{2}} \left[|a_k\rangle \pm \frac{|\phi_s(k)\rangle}{\Delta(k, \phi_1, \phi_2)} \right], \quad (4)$$
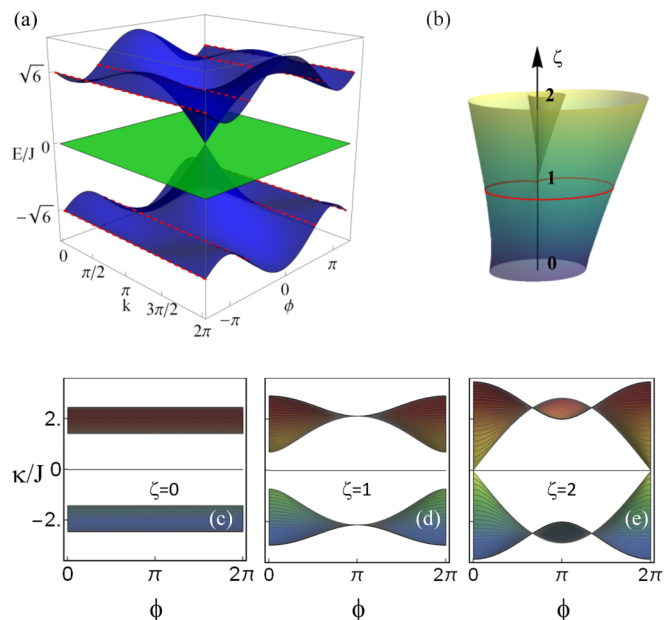

FIG. 2. (a) Spectrum of $\mathcal{H}(k, \phi_1, \phi_2)$ for $J_i = J$ with $i \in (1, 2, t1, t2)$ and $\phi_1 = \phi_2 = \phi$. The red dashed lines show the ϕ values that give four flat bands. (b) Cylindrical plot of the surface $\rho(\phi, \zeta) = 1 + \zeta \cos(\phi)$. (c)–(e) Spectrum support on the (κ, ϕ) plane for different values of ζ. They are obtained by projecting the 3D bands on the (κ, ϕ) plane.

with longitudinal momenta $\kappa_\pm(k, \phi_1, \phi_2) = \pm \Delta(k, \phi_1, \phi_2)$ and

$$\Delta(k, \phi_1, \phi_2) = \sqrt{|J_b(k)|^2 + |J_c(k, \phi_1)|^2 + |J_d(k, \phi_2)|^2}. \quad (5)$$

On the other hand, the states

$$|w_1\rangle = J_b^*|c_k\rangle - J_c^*|b_k\rangle, \quad (6)$$

$$|w_2\rangle = J_b^*|d_k\rangle - J_d^*|b_k\rangle, \quad (7)$$

spanning a two-dimensional noninvariant subspace of S_3, must be degenerate for all J's. These states thus yield two nondispersive modes for any ϕ_1 and ϕ_2 with longitudinal momentum $\kappa = 0$. The presence of these modes underlies an SU(2) non-Abelian gauge symmetry that has been shown to emerge in non-Abelian Thouless pumping [32].

The overall structure of the spectrum for $\phi_1 = \phi_2 = \phi$ with $J_i = J$ for $i = (1, 2, t1, t2)$ can be seen in Fig. 2(a) showing a band crossing at $(k, \phi) = (\pi, 0)$ and gaps for $\phi \neq 0$. We notice that for certain values of the coupling J and flux per plaquette *all* bands in the energy dispersion became flat, as indicated by the red dashed lines. This condition, a result of a destructive interference induced by the synthetic magnetic field, gives rise to light trapping and corresponds to the AB caging effect.

III. AHARONOV-BOHM CAGING

A peculiarity of the two-flux model is that the caging arises due to the destructive interference of waves propagating along three arms. This implies that, at variance with the standard two-arm single-flux AB cages [33], the values of ϕ_1 and ϕ_2 where the caging effect appears can be controlled

by changing the tunnel couplings J. We remark that when caging arises due to the destructive interference of waves propagating along two arms, it has to be necessarily located at $\phi_c = \pi$, i.e., the total amplitude is given by the sum of two identical terms having opposite sign. On the contrary, as stated above, in the θ lattice we find different caging conditions depending on the tunnel couplings. In particular, when all J's are equal, caging appears for $\phi_1 = \phi_2 = 2\pi/3$ and $\phi_1 = \phi_2 = 4\pi/3$, reflecting the trigonal symmetry of the unit cell. Related geometric and topological effects can be indeed found in Hamiltonians with these kinds of symmetries [34]. For arbitrary values of the J's and $\phi_1 = \phi_2 = \phi$, the k-dependent term in the dispersive bands of the spectrum features a factor $1 + 2(J_{t2}J_{t1}/J_1J_2)\cos(\phi)$ so that the condition to have dispersionless bands can be written as follows,

$$1 + \zeta\cos(\phi) = 0, \tag{8}$$

where the parameter $\zeta = 2J_{t2}J_{t1}/(J_1J_2)$ controls the weight of finite flux tunneling paths. In the Appendix we briefly outline the derivation of the caging condition in the most general case when all tunnel couplings and fluxes in a unit cell are different, recovering Eq. (8) as a special case. In Fig. 2(b) we show a cylindrical plot of the surface $\rho(\phi, \zeta) = 1 + \zeta\cos(\phi)$, where we clearly distinguish three cases: For $\zeta > 1$ we have two values of $\phi \in [0, 2\pi[$ where (8) is satisfied, i.e., the surface intersects twice the z axis, for $\zeta < 1$ the caging condition is never fulfilled, while for $\zeta = 1$ (8) admits only the solution $\phi = \pi$ as in the case of the standard two-arm AB caging.

To further analyze how caging arises when $\phi_1 = \phi_2 = \phi$, in Figs. 2(c)–2(e) we show the evolution of the quasienergy spectrum support as ζ increases from $\zeta = 0$ to $\zeta = 2$. At $\zeta = 0$, corresponding to $J_{t1}J_{t2} = 0$, the spectrum is clearly ϕ independent; as we increase ζ we find a pseudolocalization region around $\phi = \pi$ that evolves in a fully localized spectrum for $\zeta = 1$; eventually for $\zeta > 1$, the spectrum support shows two nodes, signaling the emergence of genus 2 AB caging. Notice that couplings among adjacent sites arise because of the presence of a mode in each guide and can be determined based on the waveguide parameters. They strongly depend on the separation between the waveguides, the dielectric constants of their core, and on the shape and dimension of the guide cross section, giving the possibility to be tuned in a wide range and then allowing us to achieve the desired ζ values in real systems. This tunability can be made dynamical by exploiting the effective refractive index modulation, enabled, for example, by phase change materials [35].

Let us now consider the light dynamics in the different caging regimes. As discussed by several authors (see e.g., Refs. [33,36]), assuming evanescent coupling of single-mode waveguides, it is described by the following coupled mode equations,

$$\begin{cases} i\partial_z a_n = J_1 b_n + J_2 b_{n-1} + J_{t1}(e^{i\phi_1}c_n + e^{-i\phi_2}d_n) \\ \qquad\quad + J_{t2}(c_{n-1} + d_{n-1}), \\ i\partial_z b_n = J_1 a_n + J_2 a_{n+1}, \\ i\partial_z c_n = J_{t1}e^{-i\phi_1}a_n + J_{t2}a_{n+1}, \\ i\partial_z d_n = J_{t1}e^{i\phi_2}a_n + J_{t2}a_{n+1}, \end{cases} \tag{9}$$

where ∂_z indicates the partial derivative with respect to z. Solving numerically the above equations on a finite lattice

with N unit cells ($4N$ sites) and open boundary conditions yields the results shown in Figs. 3 and 4.

In Fig. 3 we simulate the propagation of a light beam injected at $z = 0$ in a θ lattice consisting of N unit cells, $4N$ waveguides, with homogeneous tunnel couplings $J_i = J$ and fluxes $\phi_1 = \phi_2 = \phi = 2\pi/3$. For these parameters the dispersive bands $\kappa_\pm$ become flat and, independently of the precise position and energy of the incoming beam, light gets trapped on a cluster of few waveguides. Only the structure of the caging cluster depends on the initial condition. This is due to the fact that, depending on the initial condition, different localized bands enter the dynamics. When the light is injected in a site A of a cell n, A_n, only the upper and lower bands are dynamically occupied; caging then implies that only the waveguide A_n and the six surrounding waveguides b_n, c_n, d_n and $b_{n-1}, c_{n-1}, d_{n-1}$ are populated as shown in Fig. 3(a). The wavelength λ_0 of the oscillations between the upper and lower bands is clearly given by the inverse of the spectral gap, i.e., $\lambda_0 = 1/(2\Delta_0)$ with $\Delta_0 = \Delta(k, 2\pi/3, 2\pi/3) = \sqrt{6}J$. A somewhat similar situation arises when light is injected symmetrically in the waveguides b_n, c_n, d_n, i.e., creating the initial state $|\psi_0\rangle = \frac{1}{\sqrt{3}}(|b_{n_0}\rangle + |c_{n_0}\rangle + |d_{n_0}\rangle)$. The peculiar structure of the initial state implies that in this case, shown in Fig. 3(b), the light beam undergoes oscillations between the cell n and $n + 1$ along z without modifying its shape. Eventually in Fig. 3(c) we show the propagation of a light beam injected from the site c_n. In this case the evolution involves also the degenerate bands and the signal spreads over three unit cells.

When the caging condition is not fulfilled, light spreads to the entire lattice. This situation is considered in Fig. 4
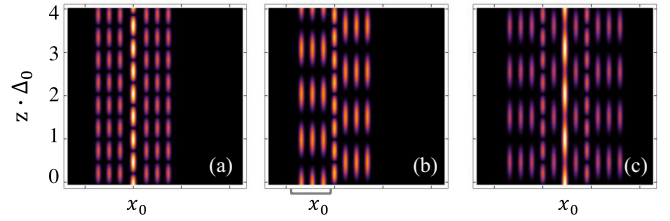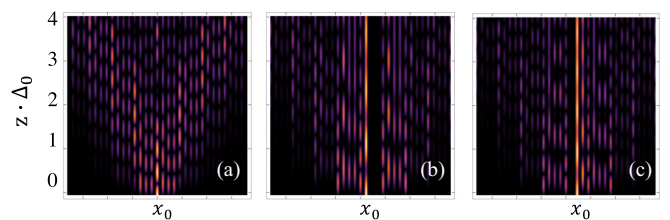

FIG. 3. Light dynamics in the presence of AB caging for three different injection configurations: (a) $|\psi_0\rangle = |a_{n_0}\rangle$, (b) $|\psi_0\rangle = \frac{1}{\sqrt{3}}(|b_{n_0}\rangle + |c_{n_0}\rangle + |d_{n_0}\rangle)$, and (c) $|\psi_0\rangle = |c_{n_0}\rangle$. Lattice parameters: $J_1 = J_2 = J_{t1} = J_{t2} = J$, $\phi_1 = \phi_2 = \phi = 2\pi/3$, $\Delta_0 = \sqrt{6}J$, $N = 40$, $n_0 = 20$.

FIG. 4. Dispersive light dynamics for $\phi_1 = \phi_2 = \phi = \pi$, i.e., away from the AB caging condition, for three different injection configurations: (a) $|\psi_0\rangle = |a_{n_0}\rangle$, (b) $|\psi_0\rangle = |b_{n_0}\rangle$, and (c) $|\psi_0\rangle = |c_{n_0}\rangle$. Other lattice parameters as in Fig. 3.

where we set $\phi_1 = \phi_2 = \pi$ and the other parameters as in Fig. 3. These values of the fluxes are special under many respects: First, as discussed in the following section, they yield [Fig. 4(a)] a weaker dispersion as compared, e.g., to the case $\phi_1 = \phi_2 = 0$, and second, they yield destructive Aharonov-Bohm interference on specific sites of the array. For example, as shown in Fig. 4(b), for a b-type injection waveguide, the propagation does not involve the sites c and d in the same plaquette, while, as shown in Fig. 4(c), for a c-type injection waveguide, the propagation does not involve the site b in the same plaquette. This is due to the fact that, at $\phi_1 = \phi_2 = \pi$, there are two tunneling paths from b to c and from b to d having opposite signs and equal amplitudes.

IV. SIGNATURES OF AHARONOV-BOHM INTERFERENCE IN THE DIFFRACTION PATTERNS

Beside inducing AB caging, synthetic gauge fields modulate light propagation in photonic lattices through AB interference, mimicking the action of their electromagnetic counterparts and yielding synthetic-flux-dependent diffraction effects. The purpose of the present section is to highlight how these effects arise in the θ lattice. To characterize diffraction for different values of the synthetic fluxes we will focus on two quantities, namely, the inverse participation number P^{-1}, defined as

$$P^{-1} = \sum_x |\Psi_x|^4, \tag{10}$$

where Ψ_x denotes the field's amplitude at position $x = na$ along the lattice, with a the lattice period, and the average square width W^2, defined as

$$W^2 = \frac{\langle x^2 \rangle - \langle x \rangle^2}{N^2}, \tag{11}$$

with $\langle x^\alpha \rangle = \sum_x x^\alpha |\psi_x|^2$. The inverse participation number is always smaller than or equal to 1 and it gives a measure of the number of sites where photons are confined, so specifically we have $P = 1$ when light is confined to a single waveguide and $P \sim m$ when light is confined to a cluster of m waveguides. The average width W is useful to characterize how the signal disperses: It equals zero in the presence of caging and in standard photonic waveguide lattices it grows as z^2. In Fig. 5(a) we plot the participation ratio as a function of z and ϕ for a θ lattice with homogeneous tunnel couplings and fluxes, i.e., $\phi_i = \phi$ and $J_i = J_{ti} = J$ with $i = 1, 2$. We assume that the system is initially prepared in the fully localized state $|a_{n_0}\rangle$, so at $z = 0$ we thus have $P^{-1} = 1$ independently of ϕ. As z increases, light starts dispersing and we clearly see the emergence of two peaks at $\phi = 2\pi/3$ and $\phi = 4\pi/3$ due to AB caging. We also notice that P^{-1} has a strongly oscillating behavior with z that is associated with dynamic oscillations between different bands. The presence of these oscillations may hinder the characterization of the different interference regimes by simply measuring the amplitude of the fields in a small cluster of sites for a given propagation length $z = \bar{z}$. For this purpose, the square width W^2 defined in (11) may be more appropriate, as we show in Fig. 5(b). There, we notice in particular the emergence of a smooth double-well structure associated with AB interference. In Figs. 5(c) and 5(d) we
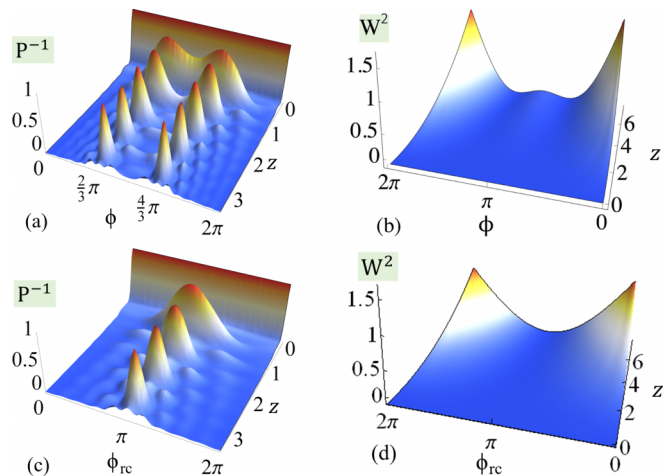

FIG. 5. (a) Inverse participation ratio P^{-1} and (b) average width W, as functions of z and ϕ. Other lattice parameters as in Fig. 3. (c), (d) Same quantities for the rhombi chain.

show the inverse participation number P^{-1} and the average width W for the rhombi chain. In this case we observe, as expected, the emergence of a single peak for P^{-1} and a single valley for W^2, at $\phi_{rc} = \phi_c$.

Having a monotonic behavior as a function of z, W can be used to characterize the different diffraction regimes for different values of the synthetic fluxes and J's. This is what we do, for the θ lattice, in Figs. 6(a) and 6(b) to illustrate the tunability of the caging effect. In Fig. 6(a) we show a density plot of the width W calculated at $zJ = 10$ for the system initially prepared in the state $|a_{n_0}\rangle$, as a function of ϕ_1 and ϕ_2 for homogeneous tunnelings. We clearly see that the contour $W = 0.5$ represented by the dashed black line essentially allows us to distinguish between a weakly dispersing region including the caging points $\phi_1 = \phi_2 = 2\pi/3$ and $\phi_1 = \phi_2 = 4\pi/3$ and a strongly dispersing region for $\phi \lesssim \pi/2$. In Fig. 6(b) we plot $W_{zJ=10}$ as a function of ϕ and J_{t2} setting all other tunnel couplings to J. In this figure the black dashed line indicates the caging condition given by (8). We notice that when J_{t2} becomes much larger than J the tunability essentially disappears, and this is due to the fact that increasing J_{t2} corresponds to a decrease of the weight of interference paths going through the site b bringing the lattice back to the single-flux regime.
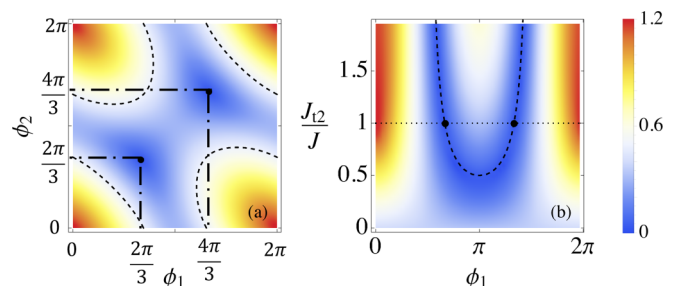

FIG. 6. Density plot of the width W as a function of ϕ_1 and ϕ_2 and as a function of J_{t2} and $\phi = \phi_1 = \phi_2$.

V. CONCLUSIONS

We presented a theoretical study of transport of light in a strip of θ-shaped plaquettes subject to synthetic magnetic fields. With respect to previous proposals, as, for example, the simple rhombi chain, the present one with three arms and two fluxes per plaquette allows us to obtain different regimes where all the energy bands became nondispersive. This allows us to realize Aharonov-Bohm cages that prevent the photon beam from escaping from finite clusters and with suitably chosen fluxes and input configurations to tune the cage size. As a second relevant result of our work, we show that it is possible to analyze the AB effect in photonic lattices by the study of the average square width W^2 as a function of fluxes or coupling values.

The caging effect and dispersion management in our waveguide system might suggest similarities with the well-known phenomenon of dispersion-controlled optical solitons [37], but they are different both in the origin and result. For dispersion-controlled optical solitons the localization of the field energy in space is due to nonlinearity, while the linear AB caging is a topological effect.

The observation of AB cages for light can be achieved using, as realistic platforms, femtosecond laser written waveguides arrays in fused-silica samples. As discussed in detail in Ref. [32], these give a high degree of control in structuring the lattice, allowing us to realize complex structures as well as tuning the nearest-neighbor couplings, and varying the speed of the writing laser beam. Complex-valued effective couplings can be realized by a proper modulation of the propagation constants [12] and by circularly bending the waveguides along the propagation direction [26,33]. These protocols lead to a nonzero magnetic flux per plaquette and allow us to study the evolution of an input state localized on specific lattice sites. These methods also allow us to tune the effective AB phases associated with the different tunneling paths, as shown, for example, in Refs. [26,33] where the synthetic magnetic field for light can be tuned by varying the phase of the photonic lattice parameter modulation.

For the simulations of light dynamics in the array we have considered the case where $\phi_1 = \phi_2$. Considering different flux configurations is also interesting and it may give rise to nontrivial results. This will be the subject of a further work with particular attention to the case $\phi_1 = -\phi_2$ that would correspond to a vanishing flux in the two-arm single-flux limit. The topology of this case is analogous to that explored in the celebrated experiment of Tonomura *et al.* [18,38] designed to provide a loophole-free test of AB prediction. In this case, as shown in the Appendix, the caging condition cannot be fulfilled and other signatures of Aharonov-Bohm interference should be identified. Our results have relevance for the fundamental properties of topological lattice and various applications as in nondiffractive image transmission schemes [39,40], all-optical logic gates [41], and optical data processing.

APPENDIX: GENERAL CAGING CONDITION

In this brief Appendix we derive the caging condition fulfilled by the fluxes ϕ_1 and ϕ_2 under the general assumption that all tunnel couplings within a unit cell are different, i.e., we make the replacement

$$J_c(k, \phi_1) \rightarrow J_{c1}e^{-i\phi_1} + J_{c2}e^{ik}, \tag{A1}$$

$$J_d(k, \phi_2) \rightarrow J_{d1}e^{i\phi_2} + J_{d2}e^{ik}. \tag{A2}$$

Under these assumptions the gap $\Delta(k, \phi_1, \phi_2)$ has the following general expression,

$$
\begin{aligned}
\Delta^2(k, \phi_1, \phi_2) = {} & J_1^2 + J_2^2 + J_{c1}^2 + J_{c2}^2 + J_{d1}^2 + J_{d2}^2 + 2(J_1 J_2 \\
& + J_{c1}J_{c2}\cos\phi_1 + J_{d1}J_{d2}\cos\phi_2)\cos(k) \\
& + 2(J_{c1}J_{c2}\sin\phi_1 - J_{d1}J_{d2}\sin\phi_2)\sin(k).
\end{aligned}
\tag{A3}
$$

From the above equation, one sees that the k-dependent part of the gap is given by the sum of two terms having different symmetries under inversion of k. In order to have caging both terms must be set to zero. We therefore obtain two equations that can be solved with respect to ϕ_1 and ϕ_2, arriving at the following final result:

$$\cos\phi_1 = \frac{J_{d1}^2 J_{d2}^2 - J_{c1}^2 J_{c2}^2 - J_1^2 J_2^2}{2J_{c1}J_{c2}J_1 J_2}, \tag{A4}$$

$$\sin\phi_2 = \frac{J_{c1}J_{c2}}{J_{d1}J_{d2}}\sin\phi_1. \tag{A5}$$

In Eq. (A5) we see that for $J_{d1}J_{d2} = J_{c1}J_{c2}$ caging requires $\phi_1 = \phi_2 = \phi$; in this limit Eq. (A4) reduces to Eq. (8). On the other hand, since the tunnel amplitudes are by definition positive, we see that for $\phi_1 = -\phi_2$ caging does not occur.

[1] D. Vanderbilt, *Berry Phases in Electronic Structure Theory* (Cambridge University Press, Cambridge, U.K., 2018).

[2] D. J. Thouless, M. Kohmoto, M. P. Nightingale, and M. den Nijs, Phys. Rev. Lett. **49**, 405 (1982).

[3] R. Resta, Europhys. Lett. **22**, 133 (1993).

[4] M. Z. Hasan and C. L. Kane, Rev. Mod. Phys. **82**, 3045 (2010).

[5] F. Wilczek and A. Shapere, *Geometric Phases in Physics* (world Scientific, Singapore, 1989).

[6] M. Aidelsburger, S. Nascimbene, and N. Goldman, C. R. Phys. **19**, 394 (2018).

[7] M. Aidelsburger, M. Atala, S. Nascimbene, S. Trotzky, Y.-A. Chen, and I. Bloch, Phys. Rev. Lett. **107**, 255301 (2011).

[8] M. Hafezi, S. Mittal, J. Fan, A. Migdall, and J. M. Taylor, Nat. Photonics **7**, 1001 (2013).

[9] M. Schmidt, S. Kessler, V. Peano, O. Painter, and F. Marquardt, Optica **2**, 635 (2015).

[10] M. C. Rechtsman, J. M. Zeuner, A. Tünnermann, S. Nolte, M. Segev, and A. Szameit, Nat. Photonics **7**, 153 (2012).

[11] Y. Lumer, M. A. Bandres, M. Heinrich, L. J. Maczewsky, H. Herzig-Sheinfux, A. Szameit, and M. Segev, Nat. Photonics **13**, 339 (2019).

[12] K. Fang, Z. Yu, and S. Fan, Nat. Photonics **6**, 782 (2012).

[13] N. Goldman and J. Dalibard, Phys. Rev. X **4**, 031027 (2014).

[14] C. Jörg, F. Letscher, M. Fleischhauer, and G. von Freymann, New J. Phys. **19**, 083003 (2017).

[15] E. Lustig, S. Weimann, Y. Plotnik, Y. Lumer, M. A. Bandres, A. Szameit, and M. Segev, Nature (London) **567**, 356 (2019).

[16] C. Jörg, G. Queraltó, M. Kremer, G. Pelegrí, J. Schulz, A. Szameit, G. von Freymann, J. Mompart, and V. Ahufinger, Light Sci. Appl. **9**, 150 (2020).

[17] Y. Aharonov and D. Bohm, Phys. Rev. **115**, 485 (1959).

[18] H. Batelaan and A. Tonomura, Phys. Today **62** (9), 38 (2009).

[19] T. T. Wu and C. N. Yang, Phys. Rev. D **12**, 3845 (1975).

[20] J. Vidal, R. Mosseri, and B. Douçot, Phys. Rev. Lett. **81**, 5888 (1998).

[21] J. Vidal, B. Douçot, R. Mosseri, and P. Butaud, Phys. Rev. Lett. **85**, 3906 (2000).

[22] D. Leykam, A. Andreanov, and S. Flach, Adv. Phys. X **3**, 1473052 (2018).

[23] S. Mukherjee, A. Spracklen, D. Choudhury, N. Goldman, P. Öhberg, E. Andersson, and R. R. Thomson, Phys. Rev. Lett. **114**, 245504 (2015).

[24] C. C. Abilio, P. Butaud, Th. Fournier, B. Pannetier, J. Vidal, S. Tedesco, and B. Dalzotto, Phys. Rev. Lett. **83**, 5102 (1999).

[25] M. Rizzi, V. Cataudella, and R. Fazio, Phys. Rev. B **73**, 144511 (2006).

[26] S. Mukherjee, M. Di Liberto, P. Öhberg, R. R. Thomson, and N. Goldman, Phys. Rev. Lett. **121**, 075502 (2018).

[27] M. Kremer, I. Petrides, E. Meyer, M. Heinrich, O. Zilberberg, and A. Szameit, Nat. Commun. **11**, 907 (2020).

[28] K. Ji, Z. Wen, Z. Liu, Y. Dai, K. Han, P. Gao, A. Gao, J. Bai, G. Zhang, and X. Qi, Opt. Lett. **43**, 4457 (2018).

[29] S. M. Zhang and L. Jin, Phys. Rev. Research **2**, 033127 (2020).

[30] K. Fang, Z. Yu, and S. Fan, Phys. Rev. B **87**, 060301(R) (2013).

[31] P. Zhang, D. Gallardo, S. Liu, Y. Gao, T. Li, Y. Wang, Z. Chen, and X. Zhang, Opt. Lett. **42**, 915 (2017).

[32] V. Brosco, L. Pilozzi, R. Fazio, and C. Conti, Phys. Rev. A **103**, 063518 (2021).

[33] S. Longhi, Opt. Lett. **39**, 5892 (2014).

[34] J. von Delft and C. L. Henley, Phys. Rev. Lett. **69**, 3236 (1992).

[35] Z. Gong, F. Yang, L. Wang, R. Chen, J. Wu, C. P. Grigoropoulos, and J. Yao, J. Appl. Phys. **129**, 030902 (2021).

[36] D. N. Christodoulides, F. Lederer, and Y. Silberberg, Nature (London) **424**, 817 (2003).

[37] A. Biswas, D. Milovic, and M. Edwards, *Mathematical Theory of Dispersion-Managed Optical Solitons* (Springer, Berlin, 2010).

[38] A. Tonomura, N. Osakabe, T. Matsuda, T. Kawasaki, J. Endo, S. Yano, and H. Yamada, Phys. Rev. Lett. **56**, 792 (1986).

[39] R. A. Vicencio, C. Cantillano, L. Morales-Inostroza, B. Real, C. Mejía-Cortés, S. Weimann, A. Szameit, and M. I. Molina, Phys. Rev. Lett. **114**, 245503 (2015).

[40] S. Xia, Y. Hu, D. Song, Y. Zong, L. Tang, and Z. Chen, Opt. Lett. **41**, 1435 (2016).

[41] B. Real, C. Cantillano, D. Lopez-Gonzalez, A. Szameit, M. Aono, M. Naruse, S.-J. Kim, K. Wang, and R. A. Vicencio, Sci. Rep. **7**, 15085 (2017).